DOI: 10.1002/cmdc.201200102

Structure–Activity Relationships and Mechanism of Action of Eph–ephrin Antagonists: Interaction of Cholanic Acid with the EphA2 Receptor

Massimiliano Tognolini,[b] Matteo Incerti,[a] Iftiin Hassan-Mohamed,[b] Carmine Giorgio,[b] Simonetta Russo,[a] Renato Bruni,[c] Barbara Lelli,[d] Luisa Bracci,[d] Roberta Noberini,[e] Elena B. Pasquale,[e] Elisabetta Barocelli,[b] Paola Vicini,[a] Marco Mor,[a] and Alessio Lodola*[a]

The Eph–ephrin system, including the EphA2 receptor and the ephrinA1 ligand, plays a critical role in tumor and vascular functions during carcinogenesis. We previously identified (3α,5β)-3-hydroxycholan-24-oic acid (lithocholic acid) as an Eph–ephrin antagonist that is able to inhibit EphA2 receptor activation; it is therefore potentially useful as a novel EphA2 receptor-targeting agent. Herein we explore the structure–activity relationships of a focused set of lithocholic acid derivatives based on molecular modeling investigations and displacement binding assays. Our exploration shows that while the 3-α-hydroxy group of lithocholic acid has a negligible role in recognition of the EphA2 receptor, its carboxylate group is critical for disrupting the binding of ephrinA1 to EphA2. As a result of our investigation, we identified (5β)-cholan-24-oic acid (cholanic acid) as a novel compound that competitively inhibits the EphA2–ephrinA1 interaction with higher potency than lithocholic acid. Surface plasmon resonance analysis indicates that cholanic acid binds specifically and reversibly to the ligand binding domain of EphA2, with a steady-state dissociation constant (K_D) in the low micromolar range. Furthermore, cholanic acid blocks the phosphorylation of EphA2 as well as cell retraction and rounding in PC3 prostate cancer cells, two effects that depend on EphA2 activation by the ephrinA1 ligand. These findings suggest that cholanic acid can be used as a template structure for the design of effective EphA2 antagonists, and may have potential impact in the elucidation of the role played by this receptor in pathological conditions.

Introduction

The 14 erythropoietin-producing hepatocellular carcinoma (Eph) receptors represent the largest family of receptor tyrosine kinases. The Eph receptors and their eight ephrin ligands are divided into two subclasses, A and B, depending on their affinities for one another and sequence homology. Generally, EphA receptors (EphA1–A8 and EphA10) bind to glycosylphosphatidylinositol-anchored ephrinA ligands (ephrinA1–A5), while the EphB receptors (EphB1–B4 and EphB6) interact with transmembrane ephrinB ligands (ephrinB1–B3), which have a short cytoplasmic domain.[1]

EphA and EphB receptors have a similar modular structure, consisting of a globular N-terminal ephrin binding domain, followed by a cysteine-rich region and two fibronectin type III repeats in the extracellular region. The intracellular region is composed of a juxtamembrane segment, a conserved tyrosine kinase domain (responsible for signal transduction), a sterile α motif (SAM) domain, and a PDZ binding motif, which serves as a docking site for interacting signaling proteins.[2,3]

The result of membrane localization of both ephrins and Eph receptors is their ability to transduce "reverse" signals into the cells in which the ephrins are expressed, as well as a "forward" signal into Eph receptor-expressing cells. As a consequence, the Eph–ephrin signaling system is responsible for modulation of several biological activities involving cellular contact, both during embryonic development and in adult tissues. In fact, these proteins modulate cell movements in morphogenetic processes such as gastrulation, segmentation, angiogenesis, axonal pathfinding, and neural crest cell migration.[4,5] Moreover, in the adult, they are involved in the maintenance of cellular architecture in various epithelia[6] and play key roles in neural plasticity[7] and regeneration of the adult nervous system.[8]

[a] Dr. M. Incerti, S. Russo, Prof. P. Vicini, Prof. M. Mor, Dr. A. Lodola
Dipartimento Farmaceutico, Università degli Studi di Parma
Viale delle Scienze 27/A, 43124 Parma (Italy)
E-mail: alessio.lodola@unipr.it

[b] Dr. M. Tognolini, I. Hassan-Mohamed, Dr. C. Giorgio, Prof. E. Barocelli
Dipartimento di Scienze Farmacologiche, Biologiche e Chimiche applicate
Università degli Studi di Parma
Viale delle Scienze 27/A, 43124 Parma (Italy)

[c] Dr. R. Bruni
Dipartimento di Biologia Evolutiva e Funzionale
Università degli Studi di Parma
Viale delle Scienze 11/A, 43124 Parma (Italy)

[d] Dr. B. Lelli, Prof. L. Bracci
Dipartimento di Biotecnologie, Università degli Studi di Siena
Via Fiorentina 1, 53100 Siena (Italy)

[e] Dr. R. Noberini, Prof. E. B. Pasquale
Sanford-Burnham Medical Research Institute
10901 North Torrey Pines Road, La Jolla, CA 92037 (USA)

Supporting information for this article is available on the WWW under http://dx.doi.org/10.1002/cmdc.201200102.

Increasing evidence supports the notion that the Eph–ephrin system, including the EphA2 and EphB4 receptors, plays a critical role in tumor and vascular functions during carcinogenesis. EphA2 in particular is overexpressed in many types of tumors, such as breast, prostate, urinary, bladder, skin, lung, ovary, and brain cancers[2] The modulation of EphA2 activity by recombinant proteins, such as monoclonal antibodies or soluble EphA receptor–Fc fusion proteins, has been shown to block tumor growth, metastasis, and angiogenic processes in animal models.[9] Moreover, genome-wide or kinome screens for somatic mutations in cancer have identified mutations in essentially all of the Eph receptors, suggesting that mutations affecting Eph receptor function play a role in cancer initiation or progression.[10–14] Therefore, the Eph–ephrin system is emerging as a novel target for the development of antitumorigenic and antiangiogenic therapies.[15]

The development of small molecules capable of blocking the biological activity of EphA2 represents an attractive alternative to antibodies, peptides, and recombinant proteins.[16–19] Few examples of EphA2 inhibitors targeting the intracellular kinase domain have been recently reported in the literature.[20] As these compounds block EphA2 activity by occupying the ATP binding pocket, they suffer from lack of selectivity, which limits their use as pharmacological tools in vivo. Conversely, compounds acting on the extracellular ligand binding domain of the Eph receptors have some advantages with respect to standard tyrosine kinase inhibitors, as they can block Eph receptor activity without having to penetrate the cell and have the potential to be more selective than ATP-mimicking agents.[21]

The three-dimensional structure of the EphA2–ephrinA1 complex has recently been resolved by X-ray crystallography.[22] The interaction between these two proteins is primarily mediated by the amino-terminal ligand binding domain of EphA2, which forms a large hydrophobic cavity able to accommodate a protruding loop from ephrinA1 (G–H loop, Figure 1).[23] The binding interface is dominated by van der Waals contacts between two predominantly hydrophobic surfaces and is reinforced by a few salt bridges, including the salt bridge between EphA2 Arg 103 and ephrinA1 Glu 119 (Figure 1). Despite the large binding interfaces in the EphA2–ephrinA1 complex, it has been shown that peptides of moderate size (12 amino acids), as well as small molecules, exemplified by salicylic acid derivatives such as compound 76D10 (Figure 2), can prevent Eph receptor–ephrin interactions, possibly by occupying the same EphA2 receptor cavity as the G–H loop of the physiological ephrin ligands.[24]

In our search for novel EphA2 receptor modulators, we recently screened an in-house chemical library of naturally occurring compounds, identifying the secondary bile acid (3α,5β)-3-hydroxycholan-24-oic acid (lithocholic acid, Figure 2) as a non-peptidic ligand of the Eph receptors.[25] Investigation of the mechanism of action of lithocholic acid revealed that this compound acts as a competitive antagonist of the EphA2 receptor ($K_i = 49 \pm 3$ μM). Furthermore, functional experiments showed that lithocholic acid inhibits EphA2 autophosphorylation in a dose-dependent manner and blocks PC3 prostate cancer cell rounding and retraction induced by EphA2 stimulation with ephrinA1. These results indicate that the lithocholic acid scaffold can be used to design effective EphA2 antagonists.

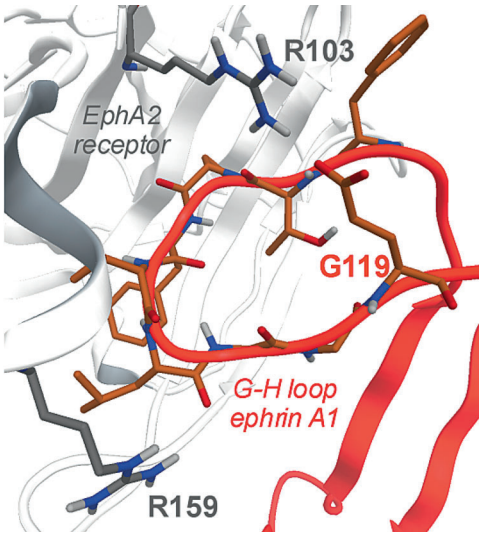

Figure 1. EphA2 ligand binding domain (white ribbons with gray side chain carbon atoms) in complex with ephrinA1 (red ribbons with orange side chain carbon atoms). The crucial salt bridge between Arg 103 (EphA2) and Glu 119 (ephrinA1) is shown.

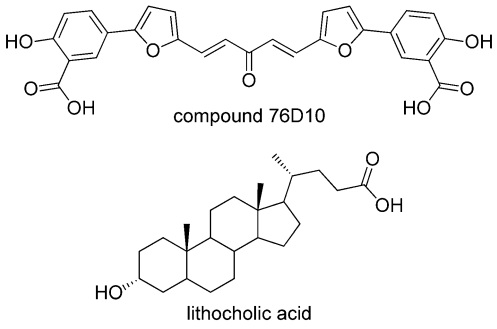

Figure 2. Recently identified antagonists of the EphA2 receptor.

We report herein the characterization of the structure–activity relationship (SAR) of (5β)-cholan-24-oic acid derivatives, leading to the identification of compounds with improved binding affinity. We performed molecular modeling studies to identify the putative binding mode of lithocholic acid (compound **1**) within the high affinity ephrin binding pocket of the EphA2 receptor. Starting from this theoretical model, a focused set of lithocholic acid derivatives, either commercially available or obtained by chemical synthesis, were examined for their ability to disrupt EphA2–ephrinA1 binding. This led to the discovery of cholanic acid, which was more potent and selective than lithocholic acid in both EphA2 binding and EphA2 phosphorylation inhibition assays.

Results and Discussion

Molecular modeling

The recent solution of the crystal structure of the ligand binding domain of the EphA2 receptor in complex with the ephrinA1 ligand[22] allowed us to investigate the binding mode of lithocholic acid to EphA2 by docking and molecular dynamics (MD) simulations. The application of these computational techniques allows us to generate working hypotheses on the recognition process involving a ligand and its receptor, aiding in the design of structural analogues.[26–30]

Figure 3a shows the best solution with regard to interaction energy (see Experimental Section) obtained by docking lithocholic acid within the high affinity ephrin binding pocket of the EphA2 receptor. The compound occupies the same space as the ephrinA1 G–H loop, inserting its cyclopenta[*a*]perhydrophenanthrene scaffold into a hydrophobic Eph receptor channel. The pentanoic acid fragment, emerging from position 17 of the lithocholic acid core, forms a salt bridge with Arg 103, mimicking the interaction with Glu 119 from ephrinA1. Finally, the 3-hydroxy group of lithocholic acid weakly interacts with Arg 159 of EphA2, which is usually engaged in a hydrogen bond with Asp 86 of ephrinA1.

To evaluate the stability of the proposed binding mode, a 30-ns MD simulation was carried out, beginning from the structure shown in Figure 3a. After a few nanoseconds of simulation, the lithocholic acid moved from its initial position to one deeper inside the EphA2 binding site, projecting its α face toward the side chain of Phe 156 (Figure 3b). The lithocholic acid hydrophobic core stably oscillated around this position until the end of the simulation (figure S1, Supporting Information), establishing van der Waals contacts with the hydrophobic surface of the receptor through the β methyl groups emerging from positions 18 and 19 of lithocholic acid (Figure 3b). These minor rearrangements of the lithocholic acid binding mode did not significantly affect the salt bridge formed by the carboxylic group of lithocholic acid with Arg 103 of EphA2, which persisted throughout the simulation (figure S2, Supporting Information). On the other hand, the interaction between the 3-hydroxy group and Arg 159 was lost in the initial phase of the MD simulation, suggesting that the contribution of this interaction to binding affinity may be negligible.

The simulation also showed that the aromatic ring of Phe 156 came into close contact with the α hydrogen atoms at positions 7 and 12 of lithocholic acid (Figure 3b), suggesting that there is limited space to introduce larger substituents at these positions. Together, these analyses suggest that the hydrophobic core of lithocholic acid can mimic the ephrin G–H loop in its interaction with the EphA2 binding site, with the carboxylic group of lithocholic acid being a fundamental component of EphA2 binding. Furthermore, the computational results also suggest that the α-hydroxy group at position 3 may not be essential for the binding activity.

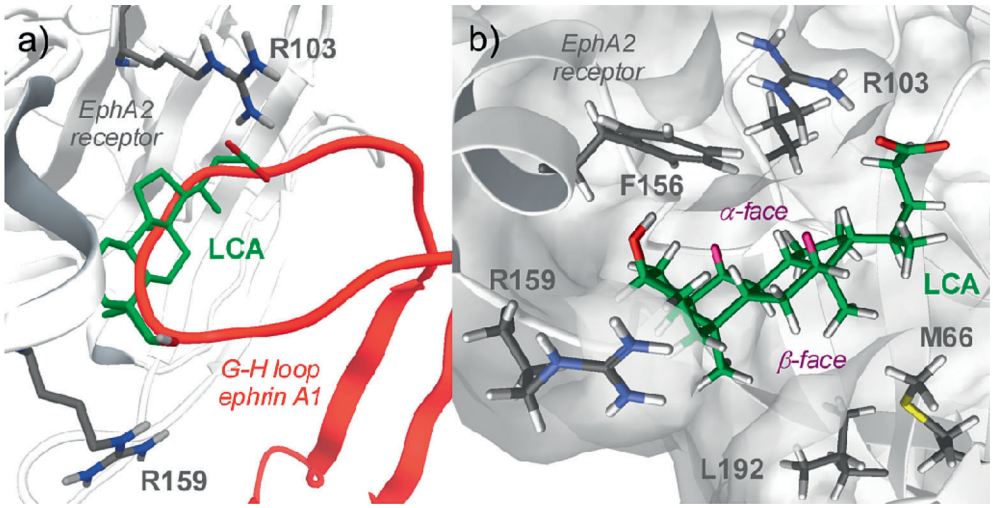

Figure 3. a) Docking of lithocholic acid (LCA, green carbon atoms) in the high-affinity ephrin binding pocket of the EphA2 receptor (white ribbons with gray side chain carbon atoms). The G–H loop of ephrinA1 is also displayed (red ribbons). b) EphA2–LCA complex obtained at the conclusion of the MD simulation. LCA carbon atoms are shown in green and hydrogen atoms in white, with the exception of those at positions 7α and 12α, highlighted in pink. The α and β faces of LCA are also highlighted. EphA2 carbon atoms are shown in gray, with white hydrogen atoms.

Structure–activity relationships of lithocholic acid derivatives

Based on the computational results reported above, 15 derivatives of lithocholic acid (compound **1**) were chosen and tested for their ability to interfere with the EphA2–ephrinA1 interaction (Table 1). Compounds **2**–**6** were selected in order to explore the interaction between the lipophilic scaffold of lithocholic acid and the EphA2 binding site. Compounds **7**–**12** and **13**–**16** were selected to examine the role played by the two polar ends of lithocholic acid. The experimental procedures employed to synthesize and characterize these compounds are reported in the Experimental Section.

The potency values corresponding to inhibition of the EphA2–ephrinA1 interaction, as indicated by the K_i values reported in Table 1, revealed that lithocholic acid derivatives are particularly sensitive to modulation of the cyclopenta[*a*]perhydrophenanthrene scaffold. Indeed, the introduction of an α-hydroxy group at positions 7 or 12 consistently results in inactivity, as exemplified by the naturally occurring cholic acid (**2**), deoxycholic acid (**3**), and chenodeoxycholic acid (**4**).[25] Similarly, introduction of a 6- or 7- keto group is detrimental to the binding affinity (compounds **5** and **6**).

Table 1. Structure–activity relationship data for lithocholic acid derivatives.

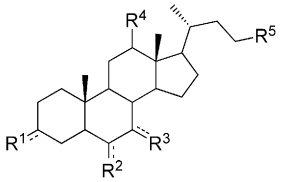

Compd	R^1	R^2	R^3	R^4	R^5	K_i [μM][a]
1	HO	H	H	H	OH	49 ± 3.0
2	HO	H	HO	HO	OH	> 200
3	HO	H	H	HO	OH	> 200
4	HO	H	HO	H	OH	> 200
5	HO	H	O	H	OH	114 ± 13
6	HO	O	H	H	OH	138 ± 20
7	O	H	H	H	OH	157 ± 47
8	O	O	H	H	OH	114 ± 14
9	H_3C O	H	H	H	OH	88 ± 11
10	HO	H	H	H	OH	25 ± 4.0
11	HO_3S	H	H	H	OH	> 200
12	H	H	H	H	OH	5.1 ± 1.4
13	HO	H	H	H	O	> 200
14	HO	H	H	H	N H OH	> 200
15	HO	H	H	H	N H NH_2	> 200
16	HO	H	H	H	OH	186 ± 27

[a] Values are the mean ± SE from a minimum of three independent experiments.

Modification of the two opposite ends of the hydrophobic core of lithocholic acid produced significant results. Oxidation of the α-hydroxy group at position 3 (compounds **7** and **8**) and acetylation of this group (compound **9**) yielded compounds with lower affinity than lithocholic acid (compound **1**). By contrast, inversion of the chiral center at position 3 yielded compound **10** ((3β,5β)-3-hydroxycholan-24-oic acid or isolithocholic acid, $K_i = 25 \pm 4$ μM), which inhibits EphA2–ephrinA1 interaction with a potency similar to compound **1**. However, when the β-hydroxy group of compound **10** was replaced by a sterically hindered substituent, the compound became inactive, as in the case of the sulfonic acid derivative **11**. The removal of the α-hydroxy group at position 3 yielded compound **12** (cholanic acid), the most potent compound of the series (Table 1 and Figure 4) which disrupts the EphA2–ephrinA1 interaction with a K_i value of 5.1 ± 1.4 μM. Together, these data indicate that position 3 of lithocholic acid projects toward a hydrophobic cavity of limited size, consistent with the binding model shown in Figure 3 b.

Finally, esterification (compound **13**), conjugation with amine derivatives (compounds **14** and **15**), or reduction to the corresponding alcohol (compound **16**) of the lithocholic acid carboxylic group yielded inactive or weakly active compounds, indicating that the presence of a negatively charged group at this position is critical for binding the EphA2 receptor.

Inhibition of EphA2–ephrinA1 by cholanic and isolithocholic acids

Of the 16 (5β)-cholan-24-oic acid analogues examined (Table 1), we further analyzed isolithocholic acid (compound **10**) and cholanic acid (compound **12**), which were found to be more potent inhibitors of EphA2–ephrinA1 interaction than lithocholic acid (compound **1**). These compounds inhibited the binding of the biotinylated ephrinA1–Fc ectodomain to the immobilized EphA2–Fc-ectodomain in a dose-dependent manner (Figure 4 a). The IC_{50} value for isolithocholic acid was 67 μM, while cholanic acid appeared to be the most potent derivative of the series ($IC_{50} = 9.6$ μM).

In addition to determining the IC_{50} values, we also determined the saturation curves for EphA2–ephrinA1 binding in the presence of increasing concentrations of isolithocholic or cholanic acid (Figure 4 b, d). We calculated the K_D or apparent K_D for each curve and drew a Schild plot, in which log [DR−1] is a function of the $-\log_{10}$[inhibitor][31] (DR = dose ratio; Figure 4 b, e). Both isolithocholic and cholanic acids yielded well-interpolated regression lines ($r^2 = 0.98$ and 0.99, respectively) with slopes of 0.96 and 0.98, respectively, indicating competitive binding. The intersection of the interpolated line with the X-axis gives a pK_i value of 4.60 (corresponding to a K_i value of 25 μM) for isolithocholic acid and 5.19 (corresponding to a K_i value of 5.1 μM) for cholanic acid. We next performed EphA2–ephrinA1 displacement experiments by incubating immobilized EphA2 with 100 μM isolithocholic acid or cholanic acid for 1 h, then washing selected wells before adding 50 ng mL^{-1} biotinylated ephrinA1–Fc. Displacement of biotinylated ephrinA1–Fc binding was observed only in the wells that were not washed, indicating that the binding of isolithocholic and cholanic acids to EphA2 is fully reversible (data not shown)

Selectivity of cholanic and isolithocholic acids for different Eph receptors

We next examined the ability of cholanic and isolithocholic acids to inhibit ephrin binding to all EphA and EphB receptors using biotinylated ephrinA1–Fc and biotinylated ephrinB1–Fc, respectively, at their K_D concentrations. In contrast to lithochol-

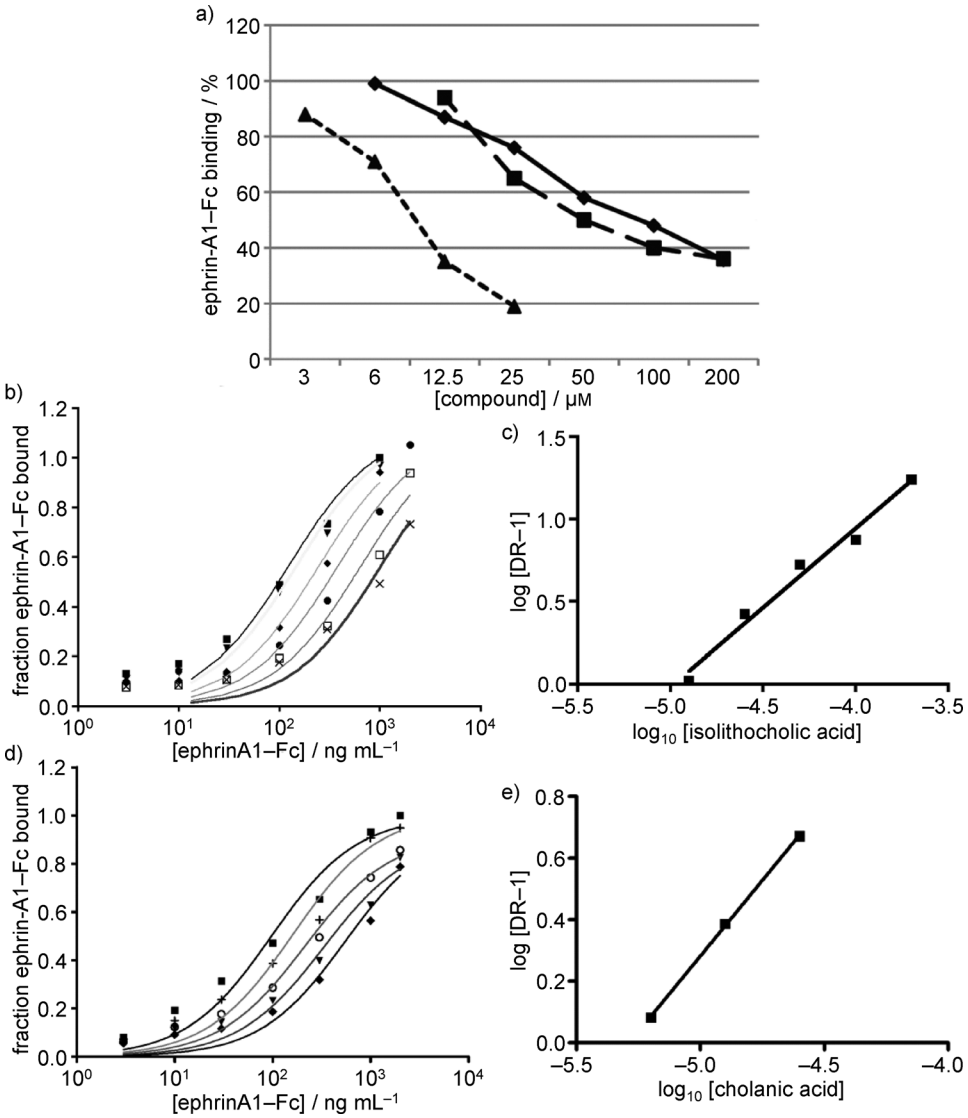

Figure 4. Isolithocholic and cholanic acid competitively inhibit EphA2–ephrinA1 binding: a) Lithocholic (◆), isolithocholic (■) and cholanic acid (▲) displace ephrinA1–Fc from the immobilized EphA2–Fc ectodomain in a dose-dependent manner. b),d) Binding of ephrinA1–Fc to immobilized EphA2–Fc in the presence of various concentrations of isolithocholic [(0 (■), 12.5 (▼), 25 (◆), 50 (●), 100 (□), and 200 μM (×)] or cholanic acid [(0 (■), 3 (+), 6 (○), 12.5 (▼), and 25 μM (◆)]. c),e) Dissociation constants (K_D) from the displacement experiments shown in panels b and d were used to calculate log [DR−1] and to graph the Schild plots for isolithocholic (slope = 0.96 ± 007) or cholanic acid (slope = 0.98 ± 002); pK_i values were estimated by the intersection of the interpolated line with the *x* axis. The slope of the interpolated line can be related to the nature of the binding. A slope between 0.8 and 1.2 indicates competitive binding, whereas a higher slope suggests nonspecific interactions (K_i = 25 ± 4 μM for isolithocholic acid; K_i = 5.1 ± 1.4 μM for isolithocholic acid).

ic acid, which we recently demonstrated to be a promiscuous ligand of all Eph receptors, cholanic and isolithocholic acids demonstrated higher selectivity for the EphA receptor subfamily. Particularly, cholanic acid displayed IC_{50} values for the EphA receptors that were 3–30-fold lower than those calculated for the EphB receptors (Figure 5). As cholanic acid was able to inhibit ephrin ligand binding to all members of the EphA receptor subfamily in the low micromolar range (3.0–7.1 μM), this suggests that cholanic acid interferes with the Eph receptor–ephrin recognition process by occupying a highly conserved region within the EphA receptor ligand binding pocket that is essential for the recruitment of ephrin ligands.

Surface plasmon resonance analysis of the binding of cholanic acid to Eph receptors

To further characterize the mechanism of action of cholanic acid, we investigated the properties of its binding to the EphA2 receptor and other proteins using a surface plasmon resonance (SPR) assay, implemented with Biacore technology.[32] The dissolved compound was injected over EphA2–Fc immobilized to surfaces attached to an optical biosensor surface, and binding was determined based on the change in mass at the sensor surface.[33] The change in mass depends linearly on the number of molecules bound; thus, SPR is a quantitative technique. Following injection, running buffer was allowed to flow over the surface, and dissociation of cholanic acid from the surface was observed. This assay enabled assessment of how cholanic acid associates and dissociates from EphA2 in real time, producing association/dissociation rate constants (k_{on}, k_{off}) as well as dissociation equilibrium constants (K_D).

As reported by SPR sensorgrams (Figure 6), cholanic acid was shown to bind the immobilized EphA2 receptor in a concentration-dependent manner. The binding was saturable and well-fitted by a 1:1 binding interaction model, confirming that the recognition process is specific. The association between EphA2 and cholanic acid was reversible, as the protein-compound complex readily dissociated, restoring the baseline signal (Figure 6).

Kinetic analysis revealed good binding parameters for cholanic acid. From the sensorgrams, it was possible to determine an association rate (k_{on}) of $4.4\times10^{4}\,M^{-1}\,s^{-1}$ and a dissociation rate (k_{off}) of $3.69\times10^{-1}\,s^{-1}$, corresponding to an affinity constant (K_D) of $8.45\times10^{-6}\,M$. This was consistent with the K_D value of $1.16\times10^{-6}\,M$ obtained from steady-state analysis (i.e., by plotting the binding at equilibrium versus the ligand con-

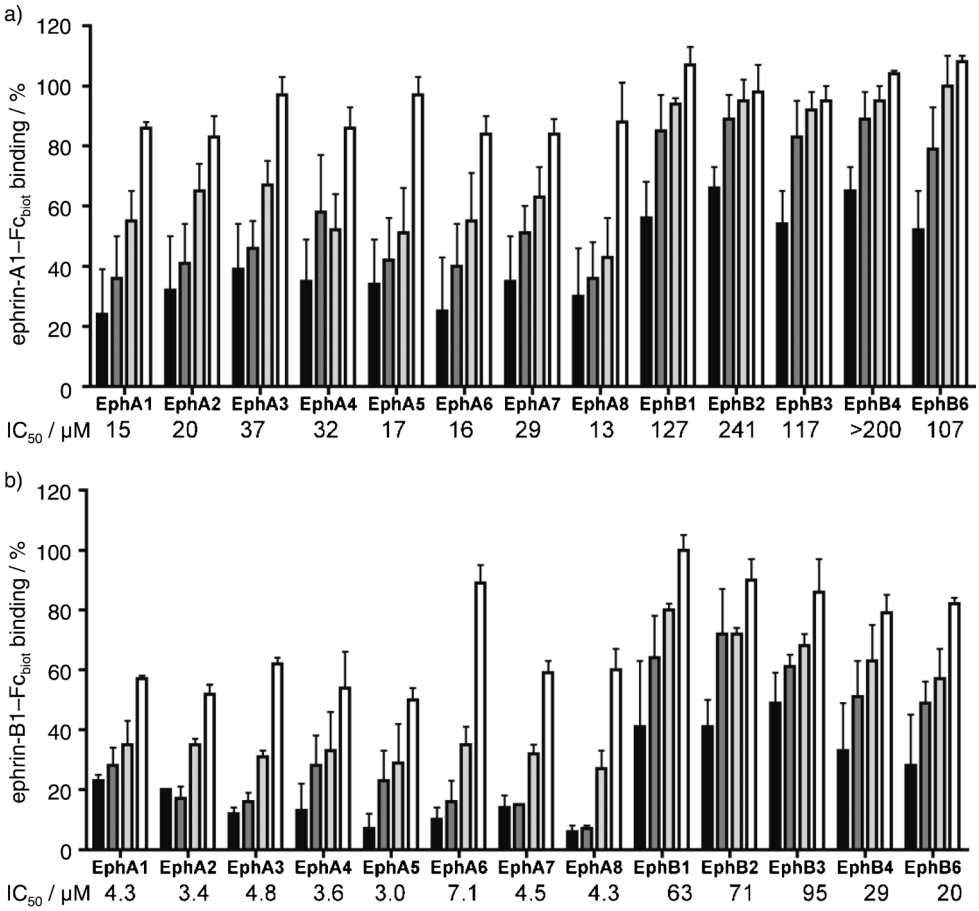

Figure 5. Lithocholic acid derivatives partially discriminate between EphA and EphB receptor subclasses: a) Isolithocholic acid and b) cholanic acid displace the binding of ephrinA1–Fc and the ephrinB1–Fc ectodomain from immobilized EphA–Fc or EphB–Fc ectodomains, respectively, in a dose-dependent manner. Tested concentrations: 3 μM (□), 10 μM (■), 30 μM (■), and 100 μM (■). IC$_{50}$ values are the means from at least three independent experiments; error bars represent standard errors.

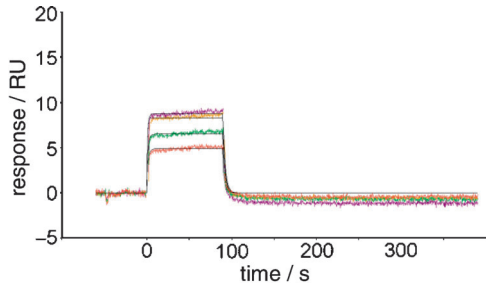

Figure 6. SPR sensorgrams for the interaction of cholanic acid with immobilized EphA2–Fc on sensor chips. The colored lines denote different cholanic acid concentrations: 3 μM (orange), 6 μM (green), 12.5 μM (pink), and 25 μM (maroon).

centration and assuming that the K_D equals the concentration which yields 50% of the maximum response,[34] figure S3, Supporting Information).

Finally, SPR analysis was applied to assess the specificity of cholanic acid for the EphA2 receptor relative to other members of the Eph–ephrin signaling system. This showed that cholanic acid at 6 μM does not bind the EphB1 receptor or the Fc-protein (figure S4, Supporting Information). Remarkably, cholanic acid binds the EphA2 receptor at this same concentration (Figure 6).

Cholanic and isolithocholic acids inhibit Eph receptor tyrosine phosphorylation at non-cytotoxic concentrations

To evaluate the functional effects of cholanic and isolithocholic acids on Eph receptors, we performed phosphorylation studies using PC3 human prostate adenocarcinoma cells, which endogenously express the EphA2 receptor, and T47D human mammary carcinoma cells, which endogenously express the EphB4 receptor. Similar to lithocholic acid, the two compounds did not stimulate Eph receptor tyrosine phosphorylation (activation) on their own (data not shown). However, they inhibited EphA2 and EphB4 phosphorylation induced by ephrinA1–Fc or ephrinB2–Fc, respectively, in a dose-dependent manner (Figure 7). The multikinase inhibitor dasatinib (1 μM), used as a control, completely blocked EphA2 phosphorylation (data not shown). According to binding data, cholanic acid inhibited Eph receptor activation induced by ephrins more potently than lithocholic acid, with IC$_{50}$ values of 12 μM (EphA2) and 38 μM (EphB4) compared with 46 and 74 μM for lithocholic acid.

Interestingly, despite the similarity between the lithocholic and isolithocholic acid binding profiles, isolithocholic acid was a more potent inhibitor of EphA2 and EphB4 phosphorylation in cells, with IC$_{50}$ values of 17 μM (EphA2) and 71 μM (EphB4). This suggests an additional inhibitory effect of isolithocholic acid on the intracellular kinase domain (see below). Compound concentrations which inhibited receptor tyrosine phosphorylation were not cytotoxic after 2 h incubation with cells (figure S5, Supporting Information).

Cholanic acid does not inhibit EphA2 kinase activity

To rule out the theory that the observed inhibition of EphA2 phosphorylation by cholanic acid was due to a direct interaction with the EphA2 kinase domain, the recombinant EphA2 kinase domain was incubated in the presence of a peptide substrate, with or without 100 μM cholanic acid. The levels of phosphorylated peptide were detected with a europium-la-

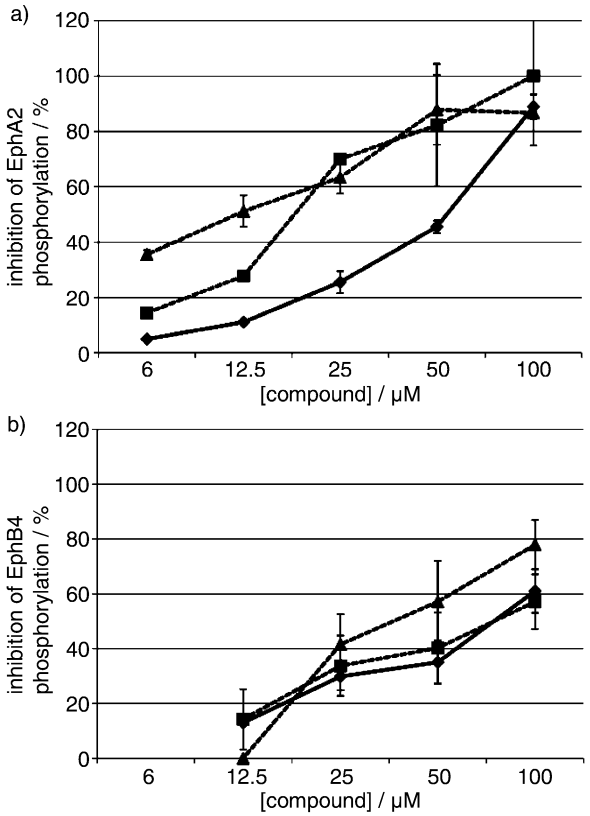

Figure 7. Lithocholic (●), isolithocholic (■), and cholanic acid (▲) inhibit Eph receptor phosphorylation in a dose-dependent manner: Inhibition of a) EphA2 phosphorylation and b) EphB4 phosphorylation. EphA2 phosphorylation was induced by 0.25 $\mu g\,mL^{-1}$ ephrinA1–Fc in PC3 cells, whereas EphB4 phosphorylation was induced with 3 $\mu g\,mL^{-1}$ ephrinB2–Fc, pre-clustered with 0.3 $\mu g\,mL^{-1}$ anti-Fc antibodies in T47D cells. Cells were pretreated for 20 min with 1% DMSO or the indicated concentrations of compounds and then stimulated for 20 min with ephrinA1/B2–Fc. Data are the means ± SE of at least three independent experiments.

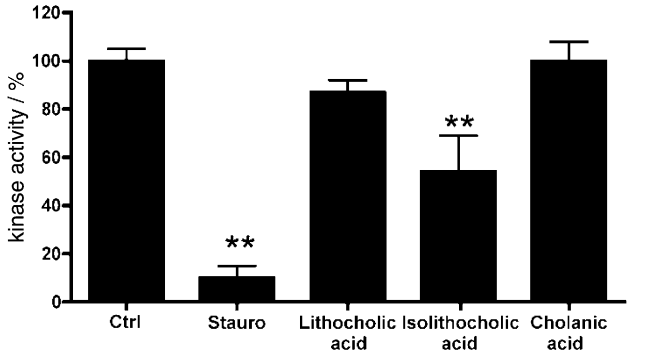

Figure 8. Cholanic acid does not inhibit EphA2 kinase activity. The enzymatic activity of the recombinant human EphA2 kinase domain was evaluated with the LANCE method using ATP and Ulight-TK peptide as substrate. EphA2 was incubated for 30 min with the indicated compounds at concentrations of 100 μM, 1 μM staurosporine, or 1% DMSO as a control; $^{**}p < 0.01$ relative to control by one-way ANOVA, followed by Tukey's multiple comparison test.

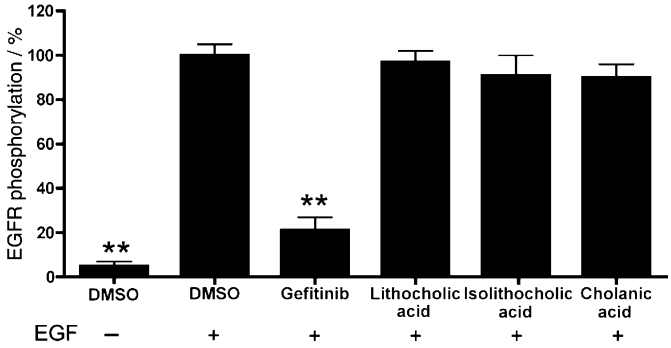

Figure 9. Isolithocholic and cholanic acids do not affect EGF receptor activity. PC3 cells were pretreated for 20 min with 100 μM lithocholic, isolithocholic, or cholanic acid, 10 μM gefitinib, or 1% DMSO as a control, and were stimulated for 20 min with 30 $ng\,mL^{-1}$ EGF. Phospho-EGF receptor levels are relative to the EGF + DMSO condition. Data are the means ± SE of at least three independent experiments; $^{**}p < 0.01$ relative to EGF + DMSO by one-way ANOVA, followed by Tukey's multiple comparison test.

beled antiphosphotyrosine antibody. Cholanic acid did not affect EphA2 kinase activity, confirming that the effect in cells is due to inhibition of Eph–ephrin protein–protein interaction. In contrast, isolithocholic acid significantly decreased EphA2 kinase activity (Figure 8), explaining the unexpectedly high potency of this compound in inhibiting EphA2 phosphorylation induced by ephrin stimulation. On the other hand, the general kinase inhibitor staurosporine fully inhibited the kinase activity of EphA2 at 100 μM (Figure 8).

The specificity of lithocholic acid as an Eph receptor antagonist was previously determined by demonstrating the lack of effects on other receptor tyrosine kinases, such as the EGF receptor, the VEGF receptor, the insulin receptor, and the insulin-like growth factor receptor 1.[25] Similar to lithocholic acid, cholanic and isolithocholic acids also did not interfere with EGF receptor activation induced by EGF at concentrations up to 100 μM (Figure 9).

Cholanic and isolithocholic acids inhibit EphA2-mediated cell retraction in PC3 cells

Cholanic and isolithocholic acids inhibited EphA2-mediated cell retraction and rounding of PC3 cells stimulated with ephrinA1–Fc at concentrations as low as 25 μM (Figure 10), suggesting that these compounds can be used to counteract the functional effects mediated by EphA2.[35] As expected, isolithocholic and cholanic acids inhibited cell retraction at concentrations similar to those required to inhibit EphA2 phosphorylation. None of the compounds affected cell morphology in the absence of ephrinA1 stimulation (Figure 10), confirming their lack of toxicity.

Conclusions

The identification of small molecules able to disrupt protein–protein interfaces is a challenging task. Complications include the presence of wide protein–protein interacting surfaces,

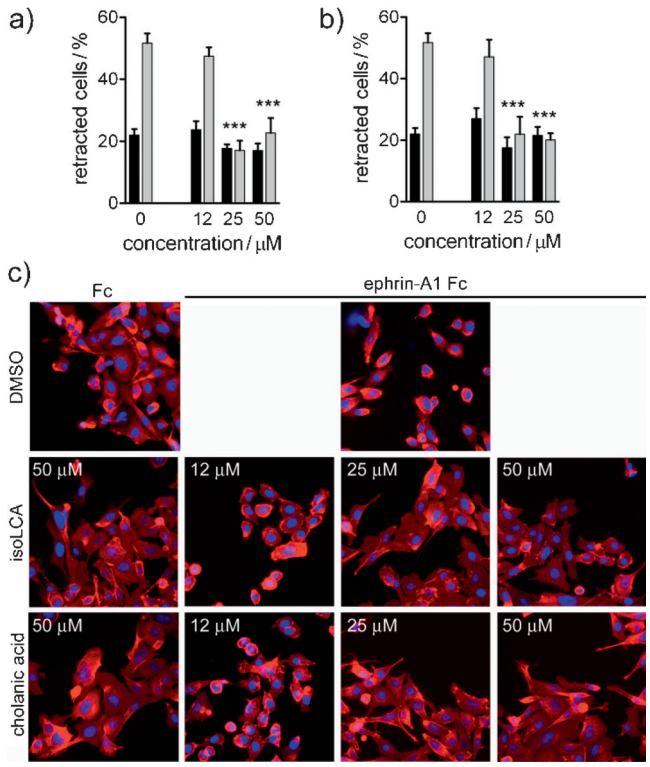

Figure 10. Inhibition of EphA2-dependent retraction and rounding of PC3 prostate cancer cells: a) Dose–response data for isolithocholic acid (isoLCA) in the presence of ephrinA1–Fc (■) using Fc (■) as a control. b) Dose–response data for cholanic acid in the presence of ephrinA1–Fc (■) using Fc (■) as a control. Histograms of panels a) and b) show the average percentage of retracting cells. Cells with a rounded shape and decreased spreading were scored as retracting. The percentages of cell retraction under various conditions were compared with those under Fc control conditions by one-way ANOVA and Dunnett's post test. c) Effects on cell morphology: PC3 cells, pretreated for 15 min with the indicated concentrations of isoLCA or cholanic acid, were stimulated with 0.5 μg mL^{-1} ephrinA1–Fc (+) using Fc as a control (−) for 20 min in the continued presence of compounds. Cells were stained with rhodamine–phalloidin to label actin filaments (red) and 4′,6-diamidino-2-phenylindole (DAPI) to label nuclei (blue); DMSO was used as a control.

which lack deep cavities where small molecules can bind with good affinity.[21] The ephrin binding pocket of the EphA2 receptor, however, seems to present favorable features for high affinity binding of small molecules, as shown here and in other recent papers.[24,35] In the present work, we report the discovery of a small molecule, cholanic acid ((5β)-cholan-24-oic acid), which binds the ligand binding domain of the EphA2 receptor with an affinity in the low micromolar range. This compound was identified through a focused medicinal chemistry effort aimed at the optimization of lithocholic acid, a weak antagonist of the Eph–ephrin system that was recently discovered by our group.[25]

A computationally driven exploration of lithocholic acid derivatives allowed us to build a clear structure–activity relationship profile and identify the stereoelectronic requirements for EphA2 binding. In particular, we found that the simultaneous presence of a large hydrophobic region (represented by the cyclopenta[*a*]perhydrophenanthrene scaffold) and an anionic hydrogen bond acceptor group (represented by a carboxylate functionality) are pivotal for effective disruption of EphA2–ephrinA1 binding, consistent with the predicted binding mode for the EphA2–lithocholic acid complex. Notably, SPR experiments indicated that cholanic acid interacts with the ligand binding domain of the EphA2 receptor, in agreement with our working hypothesis. SPR was also used to kinetically characterize the binding of cholanic acid to EphA2, yielding a steady-state binding constant in the low micromolar range ($K_D = 1.16 \times 10^{-6}$ M).

Cholanic acid competitively displaces biotinylated ephrinA1 from the EphA2 receptor. Indeed, the shift in EphA2–ephrinA1 saturation curves obtained with increasing concentration of cholanic acid produces a Schild plot consistent with competitive antagonism. The inhibitory activity of cholanic acid toward EphA2 was also confirmed by cell-based assays, where the addition of compound inhibited the ephrinA1-dependent tyrosine phosphorylation of EphA2 and retraction in PC3 cells in a dose-dependent manner. Cholanic acid is less potent in blocking the ephrinB1-dependent phosphorylation of EphB4, paralleling the results obtained in the in vitro displacement assay. Furthermore, cholanic acid has no effect on the EphA2 kinase domain, which is weakly inhibited by isolithocholic acid.

The reasonable binding affinity of cholanic acid, together with its ability to block EphA2 activity in cell lines, supports the notion that the (5β)-cholan-24-oic acid scaffold can be used as a template structure to design an improved generation of EphA2 inhibitors. On the other hand, cholanic acid suffers from high lipophilicity, which may hamper its bioavailability in vivo. However, bile acid derivatives are known to be a good reservoir of biologically active compounds, as in the case of obeticholic acid (INT-747).[36,37] This farnesoid X receptor (FXR) agonist has recently advanced to phase III clinical trials for the treatment of chronic liver diseases (clinical trial NCT00570765, study of INT-747 as monotherapy in patients with primary biliary cirrhosis). Thus, a lead optimization program aimed at the improvement of the physicochemical properties of cholanic acid may yield a small molecule able to effectively inhibit the activity of EphA2 in vivo.

Experimental Section

Molecular modeling

Molecular modeling simulations were performed, beginning from the crystal structure of the EphA2–ephrinA1 complex (3HEI.pdb),[22] using Maestro software[38] and OPLS2005 force field.[39] The EphA2–ephrinA1 complex was submitted to a protein preparation procedure which includes addition of missing side chains and hydrogen atoms, assignment of the tautomeric state of histidine residues to maximize the number of hydrogen bonds, and geometric optimization of the entire system to a root-mean-square displacement (RMSD) value of 0.3 Å.[40] At the end of this procedure, the ephrinA1 ligand was deleted from the EphA2 active site. A molecular model of lithocholic acid (**1**) was also built using Maestro, and its geometry was optimized by energy minimization using OPLS2005 to a gradient of 0.01 kcal (mol Å)$^{-1}$. Docking simulations were then performed using Glide 5.5,[41] beginning with placement of the minimized structure of lithocholic acid in an arbitrary position

within a region centered on the surface of an EphA2 channel, delimited by Arg 103, Phe 156 and Arg 159, using enclosing and bounding boxes of 20 and 14 Å on each side, respectively. van der Waals radii of the protein atoms were not scaled, while van der Waals radii of the ligand atoms with partial atomic charges lower than |0.15| were scaled by 0.8. Standard precision mode was applied. The resulting binding poses were ranked according to the G-score, and the best docking solution was selected for MD simulations. The selected EphA2–lithocholic acid docking complex was 1) solvated by ~14 000 SPC water molecules in a simulation box of 78×78×78 Å, 2) neutralized by adding 5 Na^+ ions, and 3) equilibrated by 30 ns of MD simulations. The simulation was performed in the NPT ensemble under a constant pressure of 1 atm and temperature of 300 K. All bond lengths to hydrogen atoms were constrained using M-SHAKE.[42] Short-range electrostatic interactions were cut off at 9 Å, whereas long-range electrostatic interactions were computed using the Particle Mesh Ewald method.[43] A RESPA integrator[44] was used with a time-step of 2 fs, and long-range electrostatics were computed every 6 fs. Snapshots were saved every 10 ps, for a total of 3000 structures. The MD simulation was performed with the OPLS2005 force field, using Desmond package v22623.[45]

Analysis of the MD trajectory was performed by evaluating the root mean square deviation (RMSD) of the EphA2 receptor and lithocholic acid, using the first frame of the production phase as a reference structure. For EphA2, the RMSD was measured with regard to the Cα of the amino acid residue, while for lithocholic acid, the RMSD was measured while only accounting for its heavy atoms after their optimal superposition. The interaction between the critical Arg 103 of EphA2[22] and lithocholic acid was evaluated by plotting the shortest of six possible distances between the three nitrogen atoms of the guanidinium group of Arg 103 and the two oxygen atoms of the carboxylic group of lithocholic acid for each snapshot recorded during the simulation.

Chemistry

Unless otherwise noted, reagents and solvents were purchased from commercial suppliers (Aldrich and Fluka) and were used without purification. Melting points were determined on a Gallenkamp melting point apparatus and were not corrected. Final compounds **1**–**16** were analyzed on a ThermoQuest (Italia) FlashEA 1112 Elemental Analyzer for C, H, and N. The percentages found were within ±0.4% of the theoretical values. ^{1}H NMR and ^{13}C NMR spectra were recorded on a Bruker Avance 400 spectrometer (400 MHz); chemical shifts (δ scale) are reported in parts per million (ppm). ^{1}H NMR spectra are reported in the following order: multiplicity, number of protons and approximate coupling constants (*J* value) in Hertz (Hz); signals are characterized as s (singlet), d (doublet), t (triplet), m (multiplet), br s (broad signal). Mass spectra were recorded on an Applied Biosystem API-150 EX system spectrometer with an ESI interface. Progress of reactions was monitored by thin-layer chromatography with F254 silica gel pre-coated sheets (Merck KGaA, Darmstadt, Germany). UV light and potassium permanganate solution (10% *w*/*v*) were used for detection. Flash chromatography was performed using Merck silica gel 60 (Si 60, 40–63 μm, 230–400 mesh ASTM). Tetrahydrofuran (THF) was dried by distillation over Na/benzophenone. All reactions were carried out using flame-dried glassware under a nitrogen atmosphere. Compounds **1**–**8** and **12** were purchased from Sigma and characterized by elemental analysis (see table S1, Supporting Information). Compounds **9**–**11** and **13**–**16** were synthesized according to the procedures described below.

(3α,5β)-3-Acetoxycholan-24-oic acid (9): A modification of a described procedure[46] was used (scheme S1, Supporting Information) in which lithocholic acid (**1**) (2.654 mmol) and 4-dimethylaminopyridine (DMAP) (0.409 mmol) were dissolved in anhydrous pyridine (10 mL). Acetic anhydride (21.58 mmol) was added dropwise to this solution, and the reaction mixture was stirred at room temperature under nitrogen for 3 h. Ice and water were added, then the mixture was acidified with concentrated HCl, and the white precipitate was removed by filtration and washed with water. The resulting solid was purified by flash chromatography [SiO_2, CH_2Cl_2/HCOOH/C_2H_5OH, 89:1:10 (300 mL)]. The crude product was recrystallized from EtOH and water to give **9** as a white powder (0.730 g, 65%): ^{1}H NMR (400 MHz [D_6]DMSO): δ = 0.60 (s, 3H, CH_3), 0.86 (d, 3H, *J* = 6.4 CH_3); 0.89 (s, 3H, CH_3); 0.96–1.67 (m, 26H); 1.72–1.83 (m, 4H); 1.90–1.93 (m, 1H); 1.95 (s, 3H, CH_3), 2.04–2.12 (m, 1H), 2.18–2.25 (m, 1H), 4.58–4.54 (m, 1H), 11.96 ppm (br s, 1H, OH); ^{13}C NMR (100 MHz [D_6]DMSO): δ = 12.30, 18.57, 20.88, 21.48, 23.45, 24.26, 26.40, 26.70, 27.04, 28.16, 31.14, 32.33, 34.60, 34.96, 35.26, 35.75, 41.63, 42.72, 56.02, 56.38, 73.89, 170.14, 175.25 ppm; MS (ESI) calcd for $C_{26}H_{42}O_4$: 418.61, found: 417 $[M-1]^-$.

Methyl (3α,5β)-3-hydroxycholan-24-oate (**13**): Compound **13** was synthesized following a literature protocol[47] (scheme S2, Supporting Information) in which concentrated sulfuric acid (0.5 mL) was added to a stirred suspension of lithocholic acid (**1**) (3.04 mmol) in MeOH (15 mL). The reaction mixture was stirred at room temperature for 3 h, then diluted with water. The resulting white precipitate was removed by filtration under vacuum and was washed with water. The crude product was recrystallized from EtOH and water to give **13** as a colorless solid (1.118 g, 94%): ^{1}H NMR (400 MHz $CDCl_3$): δ = 0.60 (s, 3H, CH_3); 0.85–0.91 (m, 6H), 1.02–1.98 (m, 28H), 2.17–2.36 (m, 2H), 3.57–3.64 (m, 1H), 3.67 ppm (s, 3H, CH_3); ^{13}C NMR (100 MHz $CDCl_3$): δ = 12.04, 18.26, 20.82, 23.38, 24.20, 26.42, 27.20, 28.19, 30.54, 31.00, 31.06, 34.57, 35.36, 35.84, 36.45, 40.17, 40.43, 42.10, 42.73, 43.73, 51.48, 55.95, 56.49, 71.84, 174.79 ppm; MS (ESI) calcd for $C_{25}H_{42}O_3$: 390.59, found: 413 $[M+Na^+]^+$.

Methyl (3β,5β)-3-benzoyloxycholan-24-oate (**10a**): Compound **10a** was synthesized using a modification of a described procedure[48] (scheme S3, Supporting Information) in which triphenylphosphine (0.648 mmol) was dissolved in anhydrous THF (5 mL) and cooled to 0 °C. A solution of diisopropyl azodicarboxylate (DIAD) (0.637 mmol) in anhydrous THF (1 mL) was added dropwise to the stirred solution under nitrogen, maintaining the temperature at 0 °C. After the addition was complete, the reaction mixture was warmed to room temperature and a solution of **13** (0.510 mmol) and benzoic acid (0.510 mmol) in anhydrous THF (5 mL) was added dropwise. After stirring overnight at room temperature, the solvent was removed under reduced pressure, and the residue was purified by flash chromatography [SiO_2, CH_2Cl_2/*n*-hexane from 90:10 (200 mL) to 100% CH_2Cl_2 (100 mL)]. The crude product was recrystallized from EtOH and water to give **10a** as a white powder (0.245 g, 97%): ^{1}H NMR (400 MHz $CDCl_3$): δ = 0.66 (s, 3H, CH_3), 0.92 (d, 3H, *J* = 6.4 CH_3), 1.02–1.21 (m, 9H), 1.27–1.45 (m, 9H), 1.73–2.10 (m, 11H), 2.18–2.26 (m, 1H), 2.32–2.40 (m, 1H), 3.67 (s, 3H, CH_3), 5.34 (s, 1H, OH), 7.44 (t, 2H, *J* = 7.6 Ar), 7.55 (t, 1H, *J* = 7.4 Ar), 8.05 (d, 2H, *J* = 8.4 Ar); ^{13}C NMR (100 MHz $CDCl_3$): δ = 12.08, 18.29, 21.14, 24.04, 24.20, 25.22, 26.19, 26.57, 28.19, 30.80, 31.02, 31.07, 31.09, 35.00, 35.38, 35.70, 37.74, 39.96, 40.19, 42.78, 51.48, 55.99, 56.57, 71.40, 121.31 129.51, 131.19, 132.68, 165.92, 174.77 ppm; MS (ESI) calcd for $C_{32}H_{46}O_4$: 494.70, found: 517 $[M+Na^+]^+$.

(3β,5β)-3-Hydroxycholan-24-oic acid (10): Compound **10** was synthesized following a modification of a described procedure[49] (scheme S4, Supporting Information) in which a solution of NaOH (15% *w/v*, 50 mL) was added to a solution of **10a** (1.96 mmol) in EtOH (75 mL), and the mixture was stirred at reflux overnight. EtOH was removed under vacuum, and the solution was acidified with concentrated HCl until a precipitate formed. The resulting suspension was extracted with CH_2Cl_2 (3×100 mL), and the organic extracts were washed with water and brine and dried over anhydrous Na_2SO_4. Evaporation of solvent under reduced pressure yielded a white solid that was purified by flash chromatography [SiO_2, CH_2Cl_2/HCOOH/C_2H_5OH from 99.37:0.03:0.6 (100 mL) to 97.50:0.5:2 (150 mL)]. The crude product was recrystallized from EtOH and water to give **10** as a white solid (1.02 g, 83%): ^{1}H NMR (400 MHz [D$_6$]DMSO): δ=0.60 (s, 3H, CH_3); 0.85–0.91 (m, 6H), 1.02–1.98 (m, 28H), 2.17–2.36 (m, 2H), 3.57–3.64 (m, 1H), 3.67 ppm (s, 3H, CH_3); ^{13}C NMR (100 MHz [D$_6$]DMSO): δ=12.04, 18.26, 20.82, 23.38, 24.20, 26.42, 27.20, 28.19, 30.54, 31.00, 31.06, 34.57, 35.36, 35.84, 36.45, 40.17, 40.43, 42.10, 42.73, 43.73, 51.48, 55.95, 56.49, 71.84 174.79 ppm; MS (ESI) calcd for $C_{24}H_{40}O_3$: 376.57, found: 375 $[M-1]^-$.

Methyl (3β,5β)-*S*-acetyl-3-mercaptocholan-24-oate (11a): Triphenylphosphine (0.648 mmol) was dissolved in anhydrous THF (5 mL) and cooled to 0 °C (scheme S5, Supporting Information). A solution of DIAD (0.637 mmol) in anhydrous THF (1 mL) was added dropwise to the stirred solution under nitrogen, maintaining the temperature at 0 °C. After addition was complete, the reaction mixture was warmed to room temperature, and a solution of **13** (0.510 mmol) and thioacetic acid (1.02 mmol) in anhydrous THF (5 mL) was added dropwise. After stirring overnight at room temperature, the solvent was removed under reduced pressure, and the residue was purified by flash chromatography [SiO_2, CH_2Cl_2/*n*-hexane, from 50:50 (300 mL) to 90:10 (100 mL)]. The crude product was recrystallized from EtOH and water to give **11a** as a white powder (0.148 g, 65%): mp: 128–131 °C; ^{1}H NMR (400 MHz $CDCl_3$): δ=0.63 (s, 3H, CH_3), 0.89–0.93 (m, 6H); 1.03–1.67 (m, 21H); 1.77–1.96 (m, 5H, CH_3); 2.19–2.26 (m, 1H); 2.29 (s, 3H, CH_3); 3.65(s, 3H, CH_3), 4.09 ppm (s, 1H); ^{13}C NMR (100 MHz $CDCl_3$): δ=12.05, 18.27, 20.96, 23.90, 24.17, 26.33, 26.38, 26.85, 28.17, 30.97, 31.00, 31.04, 32.01, 32.99, 35.21, 35.36, 35.72, 39.52, 40.13, 40.24, 42.73, 42.79, 51.48, 55.94, 56.49, 174.76, 195.77 ppm; MS (ESI) calcd for $C_{27}H_{44}O_3S$: 448.70, found: 471 $[M+Na^+]^+$; Anal. calcd for $C_{27}H_{44}O_3S$: C 72.27, H 9.88; found: C 72.49, H 9.53.

(3β,5β)-3-Mercaptocholan-24-oic acid (11b): Compound **11** was synthesized following a modification of a described procedure[50] (scheme S6, Supporting Information) in which a solution of NaOH (15% *w/v*, 35 mL) was added to a solution of compound **11a** (1.55 mmol) in EtOH (60 mL) and the mixture was held at reflux for 2 h under nitrogen. EtOH was removed under vacuum, and the solution was acidified with concentrated HCl until a precipitate formed. The resulting suspension was extracted with CH_2Cl_2 (3× 100 mL). The organic extracts were washed with water and brine and dried over anhydrous Na_2SO_4. Evaporation of solvent under reduced pressure yielded **11b** as a white solid that was sufficiently pure for the next reaction step (0.583 g, 96%): ^{1}H NMR (400 MHz $CDCl_3$=0.67 (s, 3H, CH_3), 0.95–1.05 (m, 6H), 1.08–1.61 (m, 22H), 1.80–2.00 (m, 6H), 2.22–2.43 (m, 3H), 3.59–3.65 (m,1H);^{13}C NMR (100 MHz $CDCl_3$): δ=12.08, 18.25, 20.93, 23.92, 24.17, 26.55, 26.72, 28.17, 28.70, 29.71, 30.24, 30.75, 31.04, 34.31, 35.31, 35.50, 35.71, 36.70, 37.46, 40.20, 40.24, 42.76, 55.96, 56.60, 180.66 ppm; MS (ESI) calcd for $C_{24}H_{40}O_2S$: 392.64, found: 391 $[M-1]^-$.

(3β,5β)-3-Sulfocholan-24-oic acid (11): A peracetic acid solution (40% *w/w*, 4.16 mmol) was added dropwise to a stirred solution of **11b** (1.27 mmol) under nitrogen at 0 °C (Scheme S7). The mixture was allowed to warm to room temperature while stirring for 4 h. Evaporation of the solvent under reduced pressure afforded a white solid that was purified by flash chromatography [SiO_2, CH_2Cl_2/HCOOH/C_2H_5OH from 83:7:10 (250 mL) to 73:7:20 (200 mL)]. The crude product was recrystallized from EtOH and water to give **11** as a white amorphous solid (0.354 g, 63%): mp: 285–288 °C; ^{1}H NMR (400 MHz [D$_6$]DMSO): δ=0.60 (S, 3H), 0.84–0.86 (m, 6H), 1.01–1.90 (m, 30H), 2.15–2.20 (m, 1H), 2.25–2.29 (m, 1H), 2.54–2.58 ppm (m, 1H); ^{13}C NMR (100 MHz [D$_6$]DMSO): δ=12.32, 18.57, 21.03, 21.37, 23.97, 24.28, 26.20, 26.74, 26.85 28.15, 31.06, 31.09, 31.56, 34.54, 35.23, 35.65, 36.36, 40.20, 42.74, 54.35, 55.94, 56.02, 56.56, 60.10, 173.70 ppm; MS (ESI) calcd for $C_{24}H_{40}O_5S$: 440.64, found: 439 $[M-1]^-$; Anal. calcd for $C_{24}H_{40}O_5S{\cdot}1.4H_2O$: C 61.61, H 9.65; found: C 61.85, H 9.62.

(3α,5β)-3-Hydroxycholan-24-hydroxamic acid (14): Compound **14** was synthesized following a modification of a described procedure[51] (scheme S8, Supporting Information) in which KOH (12.97 mmol) dissolved in MeOH (4 mL) was added dropwise to a solution of hydroxylamine hydrochloride (6.48 mmol) in MeOH (4 mL) under nitrogen at 0 °C. The mixture was stirred for a further 20 min, then a solution of **13** (0.64 mmol) in MeOH (7 mL) was added dropwise while maintaining the reaction temperature at 0 °C. The reaction mixture was then warmed to room temperature and stirred for 4 h. Finally, the mixture was diluted with water, cooled, and acidified with 6 N HCl to afford a white precipitate. The solid was removed by filtration under vacuum and purified by flash chromatography [SiO_2, CH_2Cl_2/HCOOH/C_2H_5OH from 94,50:0,5:5 (200 mL) to 82:8:10 (150 mL)]. The crude product was recrystallized from EtOH and water to give **14** as a reddish amorphous solid (0.140 g, 56%): mp: 169–173 °C; ^{1}H NMR (400 MHz [D$_6$]DMSO): δ=0.59 (s, 3H, CH_3), 0.86–0.91 (m, 6H), 1.01–1.92 (m 27H), 3.52–3.59 (m, 1H), 4.42 (s, 1H, OH), 4.42, 8.62 (s, 1H, NH), 10.30 ppm (s, 1H, OH); ^{13}C NMR (100 MHz [D$_6$]DMSO): δ=12.36, 18.69, 20.88, 23.74, 24.31, 26.63, 27.36, 28.18, 29.67, 30.85, 31.90, 34.67, 35.33, 35.62, 35.85, 36.76, 41.99, 42.73, 56.00, 56.54, 70.32, 169.94 ppm; MS (ESI) calcd for $C_{24}H_{41}NO_3$: 391.58, found: 390 $[M-1]^-$.

(3α,5β)-3-Hydroxycholan-24-hydrazide (15): Compound **15** was synthesized following a modification of a described procedure[52] (scheme S9, Supporting Information) in which hydrazine monohydrate (103 mmol) was added dropwise to a solution of **13** (0.768 mmol) in MeOH (10 mL), and the reaction mixture was stirred for 6 h at room temperature. The reaction was diluted with water, and the resulting white precipitate was removed by filtration under vacuum and washed with water. The resulting white solid was recrystallized from EtOH and water to give **15** (0.288 g, 96%): mp: 201–206 °C; ^{1}H NMR (400 MHz [D$_6$]DMSO): δ=0.59 (s, 3H, CH3), 0.85–0.91 (m, 6H), 1.01–2.04 (m 27H), 3.52–3.59 (m, 1H), 4.11 (s, 2H, NH2), 4.42 (d, 1H, J=4.4 OH), 8.88 ppm (s,1H, NH); ^{13}C NMR (100 MHz [D$_6$]DMSO): δ=12.37, 18.76, 20.90, 23.71, 24.30, 26.63, 27.40, 28.12, 30.91, 31.99, 34.71, 35.38, 35.68, 35.92, 36.85, 42.09, 42.79, 56.14, 56.61, 70.38, 172.46 ppm; MS (ESI) calcd for $C_{24}H_{42}N_2O_2$: 390.60, found: 389 $[M-1]^-$.

(3α,5β)-Cholan-3,24-diol (16): Compound **16** was synthesized following a modification of a described procedure[53] (scheme S10, Supporting Information) in which a solution of lithocholic acid (**1**) (2.66 mmol) in anhydrous THF (30 mL) was added dropwise to a suspension of $LiAlH_4$ (10.64 mmol) in anhydrous THF (30 mL), stirred at 0 °C under nitrogen. The reaction mixture was then al-

lowed to warm to room temperature and was stirred overnight. The reaction was then chilled to 0 °C and carefully quenched by dropwise addition of a 2 N H_2SO_4 solution (30 mL), then stirred at room temperature until the reaction mixture became clear. THF was removed under reduced pressure, and the mixture was extracted with diethyl ether (3×40 mL). The organic phase was washed with water and brine and dried over anhydrous Na_2SO_4. Evaporation of the solvent under reduced pressure afforded a white solid, which was recrystallized from EtOH and water to give **16** (0.791 g, 81%): ^{1}H NMR (400 MHz [D_6]DMSO): $\delta = 0.62$ (s, 3H, CH_3), 0.88–0.92 (m, 7H), 0.95–1.93 (m, 31H); 4.32 (t, 1H, $J = 6.8$ CH_2-OH), 4.44 ppm (d,1H, $J = 6.4$ OH); ^{13}C NMR (100 MHz [D_6]DMSO): $\delta = 12.31$, 18.99, 23.71, 24.30, 26.62, 27.37, 28.31, 29.59, 30.82, 32.24, 34.65, 35.57, 35.62, 35.85, 36.73, 42.00, 42.69, 56.27, 56.54, 61.75, 70.31 ppm; MS (ESI) calcd for $C_{24}H_{42}O_2$: 362.59, found: 385 $[M + Na^+]^+$.

Pharmacology

Reagents: all culture media and supplements were purchased from Lonza. Recombinant proteins and antibodies were from R&D systems. Cells were purchased from ECACC. Leupeptin, aprotinin, NP40, MTT, tween 20, BSA, and salts for solutions were from Applichem; EDTA and sodium orthovanadate were from Sigma. Human IgG Fc fragment was from Millipore (AG714).

Cell culture: PC3 human prostate adenocarcinoma cells were grown in Ham F12 supplemented with 7% fetal bovine serum (FBS) and 1% antibiotic solution. T47D human breast tumor cells were grown in RPMI 1640 with 10% FBS and 1% antibiotic solution. All cell lines were grown in a humidified atmosphere of 95% air and 5% CO2 at 37 °C.

ELISA assays and K_i/IC_{50} determinations: ELISA assays were performed as previously described.[54] Briefly, compounds (Table 1) were stocked as 20 mM solutions in dimethyl sulfoxide (DMSO) and tested both in displacement and saturation studies, starting from a concentration of 200 μM. ELISA 96-well high-binding plates (Costar #2592) were incubated overnight at 4 °C with 100 μL per well of 1 μg mL^{-1} EphA2–Fc (R&D 639-A2), diluted in sterile phosphate buffered saline (PBS: 0.2 g L^{-1} KCl, 8.0 g L^{-1} NaCl, 0.2 g L^{-1} KH_2PO_4, 1.15 g L^{-1} Na_2HPO_4, pH 7.4). The following day, wells were washed with washing buffer (PBS + 0.05% tween 20, pH 7.5) and blocked with blocking solution (PBS + 0.5% BSA) for 1 h at 37 °C. Compounds were added to the wells at selected concentrations in 1% DMSO and were incubated at 37 °C for 1 h. Biotinylated ephrinA1–Fc (R&D Systems BT602) was added at 37 °C for 4 h at a concentration corresponding to its K_D in displacement assays, or in a range from 1 to 2000 ng mL^{-1} in saturation studies. The wells were washed and incubated with 100 μL per well streptavidin-HRP (Sigma S5512) in blocking solution (0.05 μg mL^{-1} in PBS supplemented with 0.5% BSA, pH 7.4) for 20 min at room temperature, then washed again and incubated at room temperature with 0.1 mg mL^{-1} tetramethylbenzidine (Sigma T2885), reconstituted in stable peroxide buffer (11.3 g L^{-1} citric acid, 9.7 g L^{-1} sodium phosphate, pH 5.0) and 0.1% H_2O_2 (30% *w/w* in water), added immediately before use. The reaction was quenched with 3 N HCl (100 μL per well), and the absorbance was measured using an ELISA plate reader (Sunrise, TECAN, Switzerland) at 450 nm.

IC_{50} values were determined using one-site competition nonlinear regression, and K_D values of the curves with or without antagonists were calculated using one-binding site nonlinear regression analysis with Prism software (GraphPad Software Inc.). K_i values were obtained using the Schild plot,[31] in which log [DR−1] is a function of the negative $\log_{10}$ of the inhibitor concentration. The Hill coefficient was calculated using linear fitting to evaluate whether inhibition was competitive or uncompetitive.

Surface plasmon resonance (SPR): EphA2 (3000 RU), EphB1 (3000 RU), and Fc fragment (1000 RU) were immobilized via an amine group on the dextran matrix of a CM4 sensor chip, on flow cell 2, flow cell 3, and flow cell 4, respectively Blank immobilization was performed on flow cell 1 in order to be used as reference surface. Cholanic acid was dissolved into a solution of DMSO (final concentration 1 mM), then diluted to 50 μM in PBS (0.05%, pH 7.4). Subsequent dilutions from 25 μM to 3 μM were performed in 5% DMSO–PBS (0.05%, pH 7.4), which was also used as running buffer. Cholanic acid was injected over immobilized EphA2, EphB1, and Fc fragment for 90 sec at a flow rate of 30 μL min^{-1}, followed by a 300 sec dissociation. Kinetics were analyzed using Biacore T100 evaluation software and were calculated as a 1:1 binding model and as steady state affinity.

Cell lysates: PC3 or T47D cells were seeded in 12-well plates at a concentration of 105 cells per mL, 1 mL per well, in complete medium until they reached ~70% confluence and were serum-starved overnight. The following day, cells were treated with the compounds under study, vehicle, or standard drug, stimulated with the proper agonist (ephrinA1–Fc or ephrinB2–Fc), rinsed with sterile PBS, and solubilized in lysis buffer. The lysates were resuspended and rocked at 4 °C for 30 min, then centrifuged at 14000×g for 5 min. The protein content of the supernatant was measured using a BCA protein assay kit (Thermo scientific) and was standardized to 200 μg mL^{-1}.

Phosphorylation of EphA2, EphB4, and EGFR in cells: Phosphorylation of EphA2, EphB4, and EGFR was measured in cell lysates using a DuoSet IC Sandwich ELISA (R&D Systems: #DYC4056, #DYC4057, and #DYC1095, respectively) following the manufacturer's protocol. Briefly, 96-well ELISA high-binding plates (Costar #2592) were incubated overnight at room temperature with 100 μL per well of the specific capture antibody diluted in sterile PBS to the proper working concentrations. After blocking, the wells were incubated for 2 h at room temperature with 100 μL lysates per well, followed by a 2 h incubation at room temperature with the detection antibody. Receptor phosphorylation was revealed using a standard HRP format with a colorimetric reaction read at 450 nm.

EphA2 kinase assay: the ability of isolithocholic acid and cholanic acid to interact directly with the intracellular kinase domain of human EphA2 was assessed by measuring the phosphorylation of the substrate Ulight-TK peptide (50 nM) in the absence and in presence of 100 μM of the tested compound. The LANCE detection method was applied,[55] and the general kinase inhibitor staurosporine was used as a reference compound.

LDH assay: the cytotoxicity of all compounds was evaluated using the CytoTox 96 Non-Radioactive Cytotoxicity Assay following the manufacturer's protocol (Promega, #1780). Briefly, cells were seeded in 96-well plates at a density of 105 cells per mL and the following day, treated with compounds or lysis buffer for 2 h. After incubation, released LDH in culture supernatants was measured using a 30 min coupled enzymatic assay, which results in the conversion of a tetrazolium salt (INT) into a red formazan product. The resulting amount of color is proportional to the number of lysed cells and is quantified using an ELISA plate reader (Sunrise, TECAN, Switzerland) at 492 nm. The results were expressed as the ratio between absorbance of the cells treated with the compounds and cells treated with lysis buffer.

Retraction assay: The procedure followed was similar to that of references [24] and [34]. Briefly, PC3 cells (4000 cells per well) were plated in 96-well plates (Greiner Bio One, Frickenhausen, Germany) and grown for 17 h. The cells were starved for 1 hour in serum-free RPMI, incubated for 15 min with the compounds or DMSO, and stimulated for 10 min with 0.5 $\mu g\,mL^{-1}$ ephrinA1–Fc or Fc as a control. The cells were then fixed for 15 min in 4% formaldehyde in PBS, permeabilized for 3 min in 0.5% Triton X-100 in TBS, and stained with rhodamine-conjugated phalloidin (Invitrogen). Nuclei were labeled with DAPI. Cells were photographed under a fluorescence microscope, and the number of retracted cells was counted in a blinded manner.

Acknowledgements

The work was supported by the Ministero della Università e della Ricerca "Futuro in Ricerca" program (project code: RBFR10FXCP), Associazione Italiana per la Ricerca sul Cancro (AIRC) "My first AIRC" grant program (project code: 6181), and NIH grant CA138390.

Keywords: drug design · protein–protein interactions · steroids · structure–activity relationships · surface plasmon resonance

[1] N. W. Gale, G. D. Yancopoulos, *Cell. Tissue Res.* **1997**, *290*, 227 – 241.
[2] J. Wykosky, W. Debinski, *Mol. Cancer Res.* **2008**, *6*, 1795 – 1806.
[3] K. Kullander, R. Klein, *Nat. Rev. Mol. Cell. Biol.* **2002**, *3*, 475 – 486.
[4] E. B. Pasquale, *Cell* **2008**, *133*, 38 – 52.
[5] E. B. Pasquale, *Nat. Rev. Mol. Cell Biol.* **2005**, *6*, 462 – 475.
[6] H. Miao, B. Wang, *Int. J. Biochem. Cell Biol.* **2009**, *41*, 762 – 770.
[7] R. Klein, *Nat. Neurosci.* **2009**, *12*, 15 – 20.
[8] J. Du, C. Fu, D. W. Sretavan, *Curr. Pharm. Des.* **2007**, *13*, 2507 – 2518.
[9] B. Mosch, B. Reissenweber, C. Neuber, J. Pietzsch, *J. Oncol.* **2010**, *2010*, 135285.
[10] L. Ding, G. Getz, D. A. Wheeler, E. R. Mardis, M. D. McLellan, K. Cibulskis, C. Sougnez, H. Greulich, D. M. Muzny, M. B. Morgan, L. Fulton, R. S. Fulton, Q. Zhang, M. C. Wendl, M. S. Lawrence, D. E. Larson, K. Chen, D. J. Dooling, A. Sabo, A. C. Hawes, H. Shen, S. N. Jhangiani, L. R. Lewis, O. Hall, Y. Zhu, T. Mathew, Y. Ren, J. Yao, S. E. Scherer, K. Clerc, G. A. Metcalf, B. Ng, A. Milosavljevic, M. L. Gonzalez-Garay, J. R. Osborne, R. Meyer, X. Shi, Y. Tang, D. C. Koboldt, L. Lin, R. Abbott, T. L. Miner, C. Pohl, G. Fewell, C. Haipek, H. Schmidt, B. H. Dunford-Shore, A. Kraja, S. D. Crosby, C. S. Sawyer, T. Vickery, S. Sander, J. Robinson, W. Winckler, J. Baldwin, L. R. Chirieac, A. Dutt, T. Fennell, M. Hanna, B. E. Johnson, R. C. Onofrio, R. K. Thomas, G. Tonon, B. A. Weir, X. Zhao, L. Ziaugra, M. C. Zody, T. Giordano, M. B. Orringer, J. A. Roth, M. R. Spitz, I. I. Wistuba, B. Ozenberger, P. J. Good, A. C. Chang, D. G. Beer, M. A. Watson, M. Ladanyi, S. Broderick, A. Yoshizawa, W. D. Travis, W. Pao, M. A. Province, G. M. Weinstock, H. E. Varmus, S. B. Gabriel, E. S. Lander, R. A. Gibbs, M. Meyerson, R. K. Wilson, *Nature* **2008**, *455*, 1069 – 1075.
[11] T. D. Prickett, N. S. Agrawal, X. Wei, K. E. Yates, J. C. Lin, J. R. Wunderlich, J. C. Cronin, P. Cruz, S. A. Rosenberg, Y. Samuels, *Nat. Genet.* **2009**, *41*, 1127 – 1132.
[12] J. E. Ruhe, S. Streit, S. Hart, C. H. Wong, K. Specht, P. Knyazev, T. Knyazeva, L. S. Tay, H. L. Loo, P. Foo, W. Wong, S. Pok, S. J. Lim, H. Ong, M. Luo, H. K. Ho, K. Peng, T. C. Lee, M. Bezler, C. Mann, S. Gaertner, H. Hoefler, S. Iacobelli, S. Peter, A. Tay, S. Brenner, B. Venkatesh, A. Ullrich, *Cancer Res.* **2007**, *67*, 11368 – 11376.
[13] E. B. Pasquale, *Nat. Rev. Cancer* **2010**, *10*, 165 – 180.
[14] E. M. Lisabeth, C. Fernandez, E. B. Pasquale, *Biochemistry* **2012**, *51*, 1464 – 1675.
[15] M. Tandon, S. V. Vemula, S. K. Mittal, *Expert Opin. Ther. Targets* **2011**, *15*, 31 – 51.
[16] K. Lafleur, D. Huang, T. Zhou, A. Caflisch, C. Nevado, *J. Med. Chem.* **2009**, *52*, 6433 – 6466.
[17] T. Zhou, A. Caflisch, *ChemMedChem* **2010**, *5*, 1007 – 1014.
[18] B. Barlaam, R. Ducray, C. Lambert-van der Brempt, P. Plé, C. Bardelle, N. Brooks, T. Coleman, D. Cross, J. G. Kettle, J. Read, *Bioorg. Med. Chem. Lett.* **2011**, *21*, 2207 – 2211.
[19] O. P. van Linden, C. Farenc, W. H. Zoutman, L. Hameetman, M. Wijtmans, R. Leurs, C. P. Tensen, G. Siegal, I. J. de Esch, *Eur. J. Med. Chem.* **2012**, *47*, 493 – 500.
[20] Q. Chang, C. Jorgensen, T. Pawson, D. W. Hedley, *Br. J. Cancer* **2008**, *99*, 1074 – 1082.
[21] R. Noberini, I. Lamberto, E. B. Pasquale, *Semin. Cell Dev. Biol.* **2012**, *23*, 51 – 57.
[22] J. P. Himanen, Y. Goldgur, H. Miao, E. Myshkin, H. Guo, M. Buck, M. Nguyen, K. R. Rajashankar, B. Wang, D. B. Nikolov, *EMBO Rep.* **2009**, *10*, 722 – 728.
[23] J. P. Himanen, *Semin. Cell Dev. Biol.* **2012**, *23*, 35 – 42.
[24] R. Noberini, S. K. De, Z. Zhang, B. Wu, D. Raveendra-Panickar, V. Chen, J. Vazquez, H. Qin, J. Song, N. D. P. Cosford, M. Pellecchia, E. B. Pasquale, *Chem. Biol. Drug Des.* **2011**, *78*, 667 – 678.
[25] C. Giorgio, I. Hassan Mohamed, L. Flammini, E. Barocelli, M. Incerti, A. Lodola, M. Tognolini, *PLoS One* **2011**, *6*, e18128.
[26] G. E. Kellogg, M. Fornabaio, F. Spyrakis, A. Lodola, P. Cozzini, A. Mozzarelli, D. J. Abraham, *J. Mol. Graph. Model.* **2004**, *22*, 479 – 486.
[27] A. R. Leach, B. K. Shoichet, C. E. Peishoff, *J. Med. Chem.* **2006**, *49*, 5851 – 5855.
[28] A. Lodola, S. Rivara, M. Mor, *Adv. Protein Chem. Struct. Biol.* **2011**, *85*, 1 – 26.
[29] J. D. Durrant, J. A. McCammon, *BMC Biol.* **2011**, *9*, 71.
[30] A. R. King, E. Y. Dotsey, A. Lodola, K. M. Jung, A. Ghomian, Y. Qiu, J. Fu, M. Mor, D. Piomelli, *Chem. Biol.* **2009**, *16*, 1045 – 1052.
[31] O. Arunlakshana, H. O. Schild, *Br. J. Pharmacol. Chemother.* **1959**, *14*, 48 – 58.
[32] A. M. Giannetti, B. D. Koch, M. F. Browner, *J. Med. Chem.* **2008**, *51*, 574 – 580.
[33] A. Pini, A. Giuliani, C. Falciani, M. Fabbrini, S. Pileri, B. Lelli, L. Bracci, *J. Pept. Sci.* **2007**, *13*, 393 – 399.
[34] S. Núñez, J, Venhorst, C. G. Kruse, *Drug Discovery Today* **2012**, *17*, 10 – 22.
[35] R. Noberini, M. Koolpe, S. Peddibhotla, R. Dahl, Y. Su, N. D. Cosford, G. P. Roth, E. B. Pasquale, *J. Biol. Chem.* **2008**, *283*, 29461 – 29472.
[36] R. Pellicciari, S. Fiorucci, E. Camaioni, C. Clerici, G. Costantino, P. R. Maloney, A. Morelli, D. J. Parks, T. M. Willson, *J. Med. Chem.* **2002**, *45*, 3569 – 3572.
[37] C. Thomas, R. Pellicciari, M. Pruzanski, J. Auwerx, K. Schoonjans, *Nat. Rev. Drug Discovery* **2008**, *7*, 678 – 693.
[38] Maestro version 9.0, Schrödinger, LLC, New York, NY (USA), 2009.
[39] W. L. Jorgensen, D. S. Maxwell, J. Tirado-Rives, *J. Am. Chem. Soc.* **1996**, *118*, 11225 – 11236.
[40] C. Carmi, A. Cavazzoni, S. Vezzosi, F. Bordi, F. Vacondio, C. Silva, S. Rivara, A. Lodola, R. R. Alfieri, S. La Monica, M. Galetti, A. Ardizzoni, P. G. Petronini, M. Mor, *J. Med. Chem.* **2010**, *53*, 2038 – 2050.
[41] Glide version 5.5, Schrödinger, LLC, New York, NY (USA), 2009.
[42] V. Kräutler, W. F. van Gunsteren, P. H. Hünenberger, *J. Comput. Chem.* **2001**, *22*, 501 – 508.
[43] T. Darden, D. York, L. Pedersen, *J. Chem. Phys.* **1993**, *98*, 10089 – 10092.
[44] M. Tuckerman, B. J. Berne, G. J. Martyna, *J. Chem. Phys.* **1992**, *97*, 1990 – 2001.
[45] K. J. Bowers, E. Chow, H. Xu, R. O. Dror, M. P. Eastwood, B. A. Gregersen, J. L. Klepeis, I. Kolossvary, M. A. Moraes, F. D. Sacerdoti, J. K. Salmon, Y. Shan, D. E. Shaw, *Proceedings of the ACM/IEEE Conference on Supercomputing* (SC06) Tampa, FL (USA), November 11 – 17, 2006, p. 43.
[46] L. El Kihel, M. Clément, M. A. Bazin, G. Descamps, M. Khalid, S. Rault, *Bioorg. Med. Chem.* **2008**, *16*, 8737 – 8744.
[47] R. Katoch, G. K. Trivedi, R. S. Phadke, *Steroids* **1999**, *64*, 849 – 855.
[48] A. Radomińska-Pyrek, T. Huynh, R. Lester, J. St. Pyrek, *J. Lipid Res.* **1986**, *27*, 102 – 113.
[49] B. W. Katona, C. L. Cummins, A. D. Ferguson, T. Li, D. R. Schmidt, D. J. Mangelsdorf, D. F. Covey, *J. Med. Chem.* **2007**, *50*, 6048 – 6058.
[50] L. K. Steinrauf, B. Cox, E. Foster, A. Sattar, R. T. Blikenstaff, *J. Pharm. Sci.* **1978**, *67*, 1739 – 1743.

[51] K. Shimizu, T. Usui, T. Fujioka, K. Yamasaki, *J. Biochem.* **1958**, *45*, 13 – 16.
[52] A. U. Siddiqui, A. H. Siddiqui, T. S. Ramaiah, *J. Heterocycl. Chem.* **1993**, *30*, 61 – 64.
[53] A. Valkonen, E. Sievänen, S. Ikonen, N. V. Lukashev, P. A. Donez, A. D. Averin, M. Lahtinen, E. Kolehmainen, *J. Mol. Struct.* **2007**, *846*, 65 – 73.
[54] I. H. Mohamed, C. Giorgio, R. Bruni, L. Flammini, E. Barocelli, D. Rossi, G. Domenichini, F. Poli, M. Tognolini, *Pharmacol. Res.* **2011**, *64*, 464 – 470.
[55] D. M. Olive, *Expert Rev. Proteomics* **2004**, *1*, 327 – 341.

Received: February 20, 2012
Revised: March 23, 2012
Published online on ■■ ■■, 0000

*M. Tognolini, M. Incerti, I. Hassan-Mohamed, C. Giorgio, S. Russo, R. Bruni, B. Lelli, L. Bracci, R. Noberini, E. B. Pasquale, E. Barocelli, P. Vicini, M. Mor, A. Lodola**

■■ – ■■

Structure–Activity Relationships and Mechanism of Action of Eph–ephrin Antagonists: Interaction of Cholanic Acid with the EphA2 Receptor

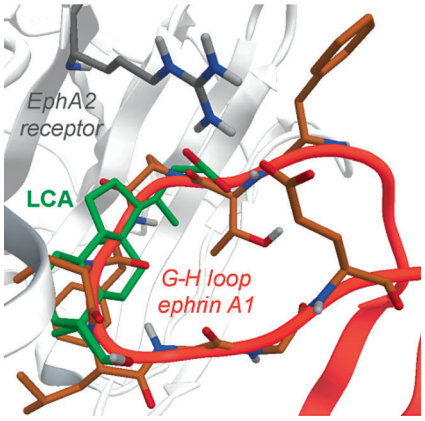

Well worth the *Eph*ort! A combined application of computational and experimental techniques led to the identification of (5α)-cholan-24-oic acid derivatives that disrupt the ephrinA1–EphA2 complex by specific interaction with the ligand binding domain of the EphA2 receptor. SAR studies provide a detailed analysis of the requirements for small molecules able to disrupt the Eph–ephrin interaction. As this system plays a critical role in tumor and vascular functions during carcinogenesis, these compounds could provide leads for therapeutic agents.

